remote sensing

MDPI

Article

Secchi Depth Retrieval in Oligotrophic to Eutrophic Chilean Lakes Using Open Access Satellite-Derived Products

Daniela Rivera-Ruiz [1,2,3,*], José Luis Arumí [1,2], Mario Lillo-Saavedra [1,4], Carlos Esse [3], Patricia Arancibia-Ávila [5], Roberto Urrutia [2,6], Marcelo Portuguez-Maurtua [7] and Igor Ogashawara [8]

1 Department of Water Resources, Universidad de Concepción, Chillán 3812120, Chile; jarumi@udec.cl (J.L.A.); malillo@udec.cl (M.L.-S.)
2 Water Research Center for Agriculture and Mining (CRHIAM), ANID Fondap Center, Universidad de Concepción, Concepción 4070411, Chile; rurrutia@udec.cl
3 Unidad de Cambio Climático y Medio Ambiente (UCCMA), Instituto Iberoamericano de Desarrollo Sostenible (IIDS), Universidad Autónoma de Chile, Temuco 478000, Chile; carlos.esse@uautonoma.cl
4 Department of Machinery and Energy, Universidad de Concepción, Chillán 3812120, Chile
5 Departamento de Ciencias, Facultad de Ciencias Básicas, Universidad del Bío-Bío, Chillán 3812120, Chile; parancib@ubiobio.cl
6 Centro de Ciencias Ambientales EULA, Facultad de Ciencias Ambientales, Universidad de Concepción, Concepción 4070411, Chile
7 Departamento de Recursos Hídricos, Facultad de Ingeniería Agrícola, Universidad Nacional Agraria La Molina, Lima 15012, Peru; mportuguez@lamolina.edu.pe
8 Leibniz-Institute of Freshwater Ecology and Inland Fisheries, 12587 Berlin, Germany; igor.ogashawara@igb-berlin.de
* Correspondence: driverar@udec.cl

Abstract: The application of the Multispectral Instrument (MSI) aboard Sentinel-2A/B constellation for assessing water quality in Chilean lakes represents an emerging area of research, particularly for the environmental monitoring of optically complex water bodies. Similarly, atmospheric correction processors applied to aquatic environments, such as the Case 2 Networks (C2RCC-Nets), are notably underrepresented. This study evaluates the capability of C2RCC-Nets using different neural networks—Case-2 Regional/Coast Color (C2RCC), C2X-Extreme (C2X), and C2X-Complex (C2XC)—to estimate Secchi depth in Lake Lanalhue (eutrophic), Lake Villarrica (oligo-mesotrophic), and Lake Panguipulli (oligotrophic). The evaluation used different statistical methods such as Spearman's correlation and normalized error metrics (nRMSE, nMAE, and nbias) to assess the agreement between satellite-derived data and in situ measurements. C2XC demonstrated the best fit for Lake Lanalhue, with an nRMSE = 33.13%, nMAE = 23.51%, and nbias = 8.57%, in relation to the median ground truth values. In Lake Villarrica, the C2XC neural network displayed a moderate correlation (r_s = 0.618) and error metrics, with an nRMSE of 24.67% and nMAE of 20.67%, with an nbias of 4.21%. In the oligotrophic Lake Panguipulli, no relationship was observed between estimated and measured values, which could be related to the fact that the selected neural networks were developed for very case 2 waters. These findings highlight the need for methodological advancements in processing satellite-derived water quality products for Chile's optical water types, particularly for very clear waters. Nonetheless, this study underscores the need for model-specific calibration of C2RCC-Nets, as lakes with different optical water types and trophic states may require tailored training ranges for inherent optical properties.

Keywords: inland waters; lake clarity; satellite remote sensing; Secchi depth; sentinel 2; water quality

Citation: Rivera-Ruiz, D.; Arumí, J.L.; Lillo-Saavedra, M.; Esse, C.; Arancibia-Ávila, P.; Urrutia, R.; Portuguez-Maurtua, M.; Ogashawara, I. Secchi Depth Retrieval in Oligotrophic to Eutrophic Chilean Lakes Using Open Access Satellite-Derived Products. *Remote Sens.* **2024**, *16*, 4327. https://doi.org/10.3390/rs16224327

Academic Editors: Emanuele Ciancia, Emanuele Organelli, Rossana Paciello and Caterina Samela

Received: 10 October 2024
Revised: 4 November 2024
Accepted: 5 November 2024
Published: 20 November 2024

1. Introduction

The spatial, spectral, and temporal resolution of freely available satellite imagery has the potential to become a valuable tool for environmental monitoring and assessment of inland waters [1]. Within the wide range of applications that can be derived from satellite

imagery, estimating water quality is of major interest, as it can complement traditional monitoring by offering a comprehensive spatial coverage and temporal frequency to study temporal trends [2]. Optical satellite data can be used to monitor water color through optically active water constituents (OACs) such as phytoplankton pigments, total suspended solids (TSS), and colored dissolved organic matter (CDOM) [3]. The water color derived from the interactions of the OACs can be used to estimate other water quality parameters such as Secchi depth and turbidity (commonly used indicators of water transparency)—a globally used proxy for water quality and ecosystem health [4,5].

Water transparency is used to assess the downwelling light attenuation (K_d), which is influenced by the absorption and scattering processes within the water column [6]. The importance of K_d—or the available light in the water column—is that it serves as a controlling factor for biological, chemical, and physical processes [7]. Thus, it is an important indicator for analyzing water quality status [8], especially due to the simplistic approach to quantify it. The traditional method used to estimate Secchi depth (SD) involves the Secchi disk: a circular black and white disk with a diameter of 20 cm that is submerged in water until no longer visible [9]. It is one of the simplest and most cost-effective methods for measuring a water quality parameter, and it is an international standard method for measuring SD and consequently water transparency. Due to its simplicity, Secchi disk measurements are typically included in most water quality monitoring programs, where extensive historical records—dating back more than 150 years—provide valuable information for assessing trends in water quality [10]. Chilean water quality programs such as the "Red Minima de Lagos" managed by the "Dirección General de Aguas" (DGA) include SD as a standard measurement, with records dating back to the 1980s for selected inland waters [11].

These extensive historical records of water clarity in Chilean inland waters open a unique opportunity to expand our understanding of water quality changes in combination with satellite imagery. The use of remote sensing technology has been growing in Chile due to its capacity to allow broader and more frequent monitoring of inland waters, complementing traditional limnological methods [4]. Most studies using satellite remote sensing for inland water quality in Chile were published in recent years, and have been used mostly to detect chlorophyll-*a* (chl-*a*) [12–18], while few studies were used for SD retrieval. Within these studies, only [12] and [18] used Sentinel 2—MSI for chl-*a* concentration retrieval, while all other studies chose the Landsat Thematic Mapper (TM), the Enhanced Thematic Mapper (ETM+), and/or the Operational Land Imager (OLI). In our literature search, only one study related SD and turbidity for several North Patagonian Lakes using Landsat 5 TM, 7 ETM+, and 8 OLI imagery [19]. Furthermore, [17] estimated chl-*a* and turbidity in a small urban lake using Landsat 8 OLI, and this is the only study that has evaluated and validated the water-leaving reflectance using in situ radiometric measurements of the water column. In this context, various aquatic atmospheric correction algorithms such as the Atmospheric Correction for OLI 'lite' (ACOLITE) [20], Image Correction for Atmospheric Effects (iCOR) [21], the Land Surface Reflectance Code (LaSRC) [22], and C2RCC [23] were used in the previous research, in which ACOLITE outperformed other aquatic atmospheric correction processors. This pre-processing of satellite images to correct for the effects of the atmosphere over aquatic systems has been recognized as an essential step for the accurate retrieval of water quality parameters from optical satellite imagery [24,25].

Despite the crucial role of aquatic atmospheric correction in enhancing the accuracy of satellite-derived products, the access to radiometric equipment, essential for validating the aquatic atmospheric correction procedure, is limited, especially in the Global South [4]. This limitation produces a need for alternative methods to promote the development of the field of remote sensing of water quality. In Chile, the use of Sentinel MSI 2A and 2B in combination with the C2RCC-Nets (C2RCC, C2X, and C2XC) is still heavily underexplored. A recent study [25] showed that C2RCC and C2X outperformed ACOLITE and iCOR in terms of atmospheric correction, especially in the near-infrared (NIR) region of the electromagnetic spectrum. Similar results were observed by [26], which compared

different atmospheric correction processors, and for the NIR region, ACOLITE was also outperformed by C2X. Thus, it is important to consider the use of these processors in Chilean waters.

This study aimed to evaluate the accuracy of the C2RCC-Nets' atmospheric correction processor and its different neural networks—C2RCC, C2X, and C2XC—for the estimation of SD in Chilean lakes with different trophic states. By using the MSI sensor onboard Sentinel 2A/B constellation, this study addresses the need for reliable and accessible monitoring tools that can complement traditional methods to support sustainable water resource management. To do this, we compared satellite-derived SD estimates using different atmospheric correction processors with in situ measurements of SD from different lakes during austral spring and summer from 2018 to 2024. The presented method offers a globally scalable alternative for regions with limited access to radiometric equipment, providing actionable methods for integrating satellite data into sustainable water management practices in remote and data-scarce environments. Ultimately, the results underscore the potential of remote sensing technology to advance our understanding of aquatic ecosystems under the pressures of climate change and anthropogenic activities.

2. Materials and Methods

2.1. Study Area

This study used the data collected in three different lakes: Lake Lanalhue, Lake Villarrica, and Lake Panguipulli, located in the Bío-Bío, Araucanía, and Los Ríos regions in South-Central Chile (Figure 1, Table 1).

Lake Lanalhue is a coastal lake located at 37°55′S and 73°18′W in the Bío-Bío Region, at an altitude of 12 m a.s.l. It has an area of 31.9 km^2, a mean depth of 13 m, and a maximum depth reaching 26 m. Lanalhue is a tectonically influenced lake that forms part of the larger Nahuelbutan Lake System. Occupying a narrow valley along the Nahuelbuta Mountain Range, the lake is located within a temperate, Mediterranean-influenced climate zone along the coast. During the summer, the lake undergoes thermal stratification, which can lead to hypoxic conditions in the bottom layers due to an increased production of organic material [27]. The surroundings of Lake Lanalhue have experienced an increase in the export of sediments and nutrients due to modifications of the hydrological regime [28]. These changes occurred due to the conversion of native forest to cultures of *Pinus radiata* and *Eucalyptus globulus.* In addition, the lake has been affected by touristic activities as well as a lack of appropriate wastewater treatments, leading to an increase in untreated discharges into the lake [27]. At present, more than 39.60% (172.49 km^2) of the catchment area is comprised by monoculture forest plantations, followed by native forest and shrub (23.16%; 100.92 km^2) and agricultural land use (15.47%; 67.40 km^2) [27].

Lake Villarrica is located at 39°25′S, 72°09′W in the Araucanía Region, situated at an elevation of over 215 m a.s.l. The lake spans a total area of 173.9 km^2, with a mean depth of 120 m and a maximum depth of 165 m. Lake Villarrica originated from natural damming by a terminal moraine left from the last glaciation. The climate in the area is temperate and rainy, which supports a temperate, monomictic lake system that undergoes stratification during summer and vertical mixing during winter [29]. The catchment area is 2884.15 km^2 with main land cover/land use consisting of urban, agricultural, and forested areas towards the valley, while native forest is still prominent towards the Andes Mountains. Previous studies showed that land use changes have occurred persistently across this region over the last 50 years, resulting in the deterioration of the water quality [30,31]. A different study [31] observed that the combination of land cover change and climate change led to an increase in nutrient input, causing an accelerated eutrophication process in the lake. This is becoming increasingly evident with the occurrence of extreme bloom events by *Dolichospermum* sp., where microcystin concentrations above 10 μgL^{-1} have been recorded [32,33]. The same could be observed in the most recent environmental reports, which indicated that the lake's trophic state is mainly oligotrophic with strong fluctuations towards mesotrophic (DGA, 2018a; 2018b).

Lake Panguipulli is located south of Lake Villarrica, at 39°43′S, 72°13′W in the Los Ríos Region, at an elevation of 130 m a.s.l. It is one of the largest lakes in the north Patagonian freshwater district in Chile, covering an area of 117 km^2, with a mean and maximum depth of 126 m and 268 m, respectively. Lake Panguipulli is of glacial origin, situated in a temperate and rainy climate. It is classified as temperate-monomictic lake, exhibiting very stable stratification during the summer [34].

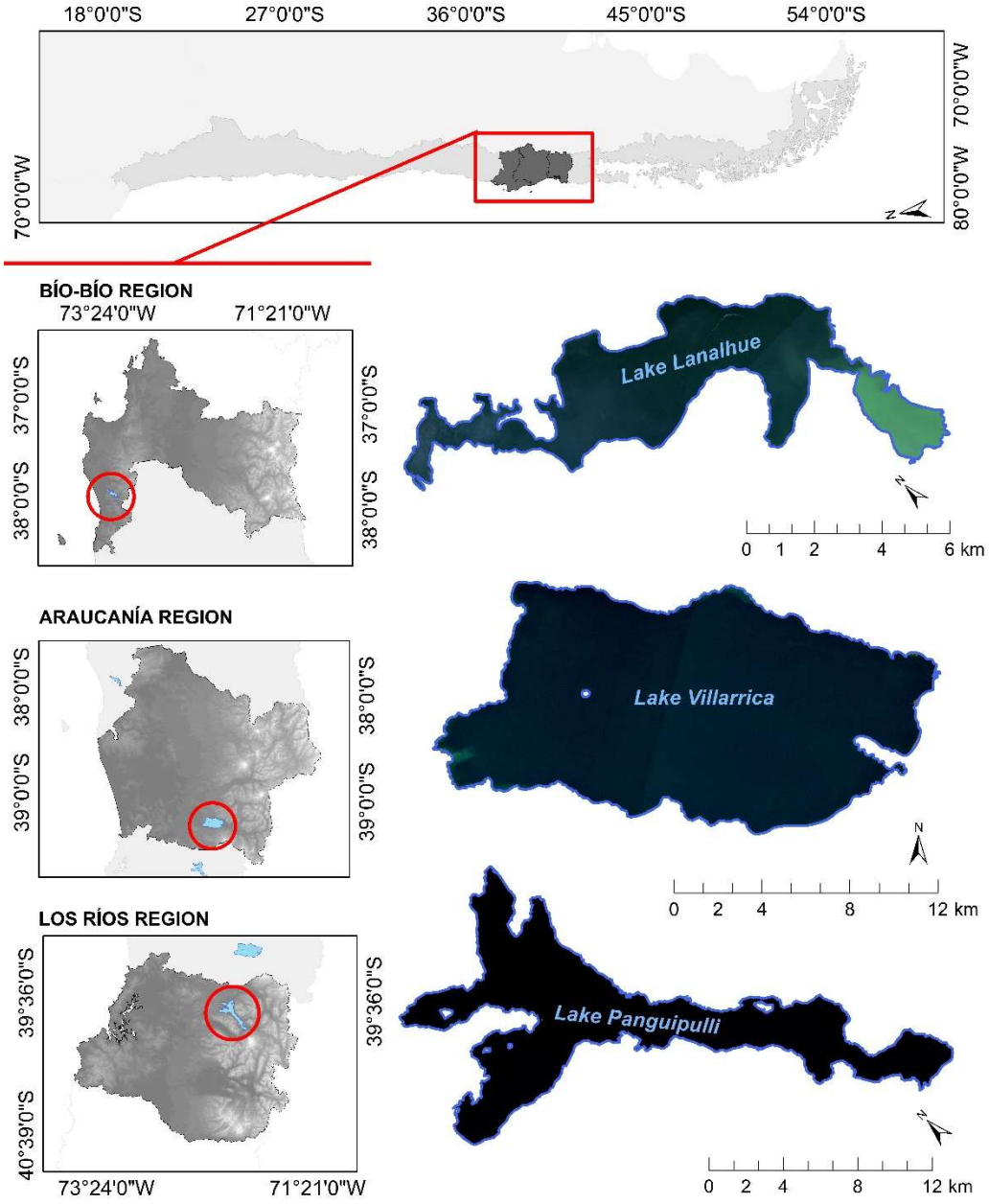

Figure 1. Locations of Lake Lanalhue, Lake Villarrica, and Lake Panguipulli (circled in red) and their respective regions in Chile.

A few years ago (late 90s, mid 2000s, and 2012), the lake was classified as mesotrophic due to its concentrations of phosphorous and chl-*a*. Nonetheless, in 2015, the lake presented oligotrophic conditions [12,35]. The catchment area expands to over 3811 km^2, predominately covered by native forest (84%) and pasture (15%), followed by small areas of agriculture, urbanization, monoculture forest plantations, and open areas [12,31].

Table 1. Geographical and limnological characteristics of Lake Lanalhue, Lake Villarrica and Lake Panguipulli.

Geography and Limnology	Lanalhue [1]	Villarrica [2]	Panguipulli [3]
Latitude South	37°55′	39°25′	39°43′
Longitude West	73°18′	72°09′	72°13′
Altitude (m a.s.l)	12	215	130
Catchment area (km^2)	438	2884	3811
Area (km^2)	31.9	173.9	117
Mean depth (m)	13	120	126
Maximum depth (m)	26	165	268
Trophic state	Eutrophic	Oligo to mesotrophic	Oligotrophic

Modified from [27] [1], [35,36] [2], and [12] [3].

2.2. Transparency and Water Quality Data

The dataset for this study focuses on SD measurements to assess water transparency and was obtained through field campaigns and the acquisition of data from secondary sources [18].

Field campaigns were timed to match up with satellite overpasses, ensuring a temporal discrepancy of no more than ±1 day and ±2 h. Monitoring activities were conducted during the summer from 2022 to 2024, on cloud-free days with wind speeds below 5 kmh^{-1} to minimize environmental interference. Lake Lanalhue was monitored in 2023 over two consecutive days (n = 22), while Lake Villarrica was monitored across all years, resulting in six campaigns. However, due to variable weather conditions, only three dates were included in this study (n = 44). Lake Panguipulli was monitored in 2023 and 2024, but only data from 2023 (n = 13) were used, due to weather constraints.

SD (in m) was obtained using a 20 cm diameter black-and-white disk, deployed from the shaded side of the boat to reduce glare and reflection errors. In addition to Secchi depth, water temperature (°C) was measured using a pH/EC/TDS/Temperature probe, model HI98129 (HANNA Instruments, Santiago, Chile).

Following the collection of primary data, secondary data were sourced from the Dirección General de Aguas (DGA, http://www.dga.cl/, accessed on 14 March 2024), which has maintained and operated the Red Mínima de Lagos with data since the 1980s. Additionally, the study incorporates data from the Sistema Nacional de Información Ambiental (SINIA, https://sinia.mma.gob.cl/, accessed on 20 March 2024) managed by the Ministerio de Ambiente (MMA), which has conducted extensive limnological studies across Chilean lakes. Technical reports resulting from this search compiled by [28,29,37–39] were thoroughly reviewed to ensure their applicability and relevance to the study. Criteria for the selection of secondary sourced data to be used in this study included that data should be collected on cloud-free days, with wind speeds < 5 kmh^{-1}, and SD and water temperature should be collected ±1 days from satellite overpass schedule. Through this process, two sampling campaigns were added for Lake Lanalhue (n = 10), five additional sampling campaigns were added for Lake Villarrica (n = 17), and six sampling campaigns were added for Lake Panguipulli (n = 13).

Given that the combined dataset was collected by multiple observers, potential variability may exist due to minor differences in observer technique. Nevertheless, both primary and secondary data measurements were collected by trained personnel, using standardized protocols. This combined dataset was used for validation (Table 2).

Table 2. Description of the validation dataset and retrieval method for Lake Lanalhue, Villarrica and Panguipulli.

Lake	Parameter *	Min	Max	Mean	Median	StdDev **
Lanalhue (n = 32)	SD (m)	0.60	5.00	2.20	2.50	1.15
	Tw (°C)	21.4	22.70	22.0	21.8	0.57
Villarrica (n = 61)	SD (m)	3.50	11.00	6.43	7.00	2.02
	Tw (°C)	15.60	25.00	21.60	21.90	1.92
Panguipulli (n = 26)	SD (m)	6.50	16.83	11.92	12.00	1.98
	Tw (°C)	17.62	23.08	20.20	20.18	1.89

* SD: Secchi depth; Tw: surface water temperature. ** StdDev: standard deviation.

2.3. Trophic State Index

To assure that the SD dataset effectively represents three different trophic conditions as described by former studies, [40] trophic state index (TSI) was calculated using SD transparency (Equation (1)) as follows:

$$\mathrm{TSI} = 60 - 14.41 \ \ln \mathrm{SD} \quad (1)$$

The values of TSI range from 0 to 100, where its simplest classification includes oligotrophic, mesotrophic, eutrophic, and hypereutrophic conditions (Table 3).

Table 3. Ranges and classifications adapted from Carlson's trophic state index with the associated SD values.

Trophic Status	TSI Range	TSI	SD (m)
Oligotrophic	<30	0	64
		10	32
		20	16
		30	8
Mesotrophic	30 < TSI < 60	40	4
		50	2
		60	1
Eutrophic	60 < TSI < 90	70	0.50
		80	0.25
		90	0.12
Hypereutrophic	90 < TSI < 100	100	0.06

2.4. Satellite Imagery

Sentinel 2 MSI Level-1C scenes from the European Space Agency (ESA) were acquired from the Copernicus Open Access Hub (https://scihub.copernicus.eu, accessed on 18 May 2024). In total, fifteen images were downloaded: three for Lake Lanalhue, eight for Lake Villarrica, and 12 for Lake Panguipulli. Tiles T18HXD and T18HYB were used to extract the scenes for Lanalhue and for Villarrica and Panguipulli, respectively. Due to Panguipulli's location, T18HYB tiles were supplemented with T18GYA to comprehensively cover the southern area of the lake (Table 4).

Table 4. Overpass schedule of Sentinel 2A/2B constellation, product identification (ID), and the temporal offset (days) from monitoring campaigns.

Lake	Tile	Satellite Overpass	Product ID	Temporal Offset (Days)
Lanalhue	T18HXD	13 February 2018	GS2A_20180213T143751_013821_N02.06	0
		18 January 2022	GS2B_20220118T143719_025433_N03.01	0
		22 February 2023	GS2B_20230222T143729_031153_N05.09	0, +1

Table 4. *Cont.*

Lake	Tile	Satellite Overpass	Product ID	Temporal Offset (Days)
Villarrica	T18HYB	25 February 2019	GS2A_20190225T142751_019212_N02.07	+1
		28 February 2019	GS2A_20190225T142751_019212_N02.07	−1
		9 February 2021	GS2B_20210209T142729_020528_N02.09	+1
		1 March 2021	GS2B_20210301T142729_020814_N02.09	+1
		4 March 2021	GS2B_20210304T143729_020857_N02.09	−1
		13 January 2023	GS2B_20230113T143719_030581_N05.09	0
		2 February 2023	GS2B_20230202T143729_030867_N05.09	0
		24 January 2024	GS2A_20240123T143741_044852_N05.10	−1
Panguipulli	T18GYA/ T18HYB	2 December 2018	GS2B_20181202T142749_009088_N02.07	+1
		31 January 2019	GS2B_20190131T142759_009946_N02.07	−1
		24 February 2021	GS2A_20210224T142731_029651_N05.00	+1
		6 November 2021	GS2B_20211106T142729_024389_N05.00	0, +1
		11 March 2022	GS2A_20220311T142741_035085_N04.00	0, −1
		18 January 2023	GS2A_20230118T143721_039561_N05.09	0

2.5. Image Processing

The Sentinel Application Platform version 9.0.0 (SNAP: http://step.esa.int/main/toolboxes/snap/, accessed 10 November 2023), a freely available software developed by Brockmann Consult GmbH, Hamburg, Germany, was used for image processing, was used in this study. SNAP facilitates the processing of Earth Observation (EO) data, offering a suite of tools for the pre-processing, analysis, and visualization of satellite imagery and products, including those specifically tailored for Sentinel 2 MSI [41]. Among its specialized capabilities, SNAP stands out as the sole platform capable to process images using C2RCC-Nets [23]. In this study, the pre-processing involved subsetting the scenes to the area of interest to reduce the demand on computer resources and processing time. Additionally, all images were resampled to a 10 m spatial resolution, a necessary step before applying C2RCC, C2X and C2XC.

The C2RCC-Nets were developed for the inversion of the water-leaving reflectance spectrum, essential for the accurate retrieval of optically significant water constituents. It employs radiative transfer simulations with neural networks (NNs) trained to encompass a wide range of scattering and absorption scenarios [23]. Within the C2RCC-Nets, three NNs are employed. The C2RCC uses the NASA bio-Optical Marine Algorithm Dataset (NOMAD) [42], and C2X is complemented with the CoastColor Round Robin (CCRR) dataset for extreme cases, covering more turbid waters [43]. Both datasets provide in situ measurements of the inherent optical properties (IOPs), Top-of-Atmosphere, and water-leaving radiances from various water types. NOMAD and CCRR are used to parameterize and validate simulations that mimic how light interacts within the water bodies. These simulations, comprising 5 million scenarios that mirror real-world examples, are used to train the NNs in the ability to predict IOPs in water from satellite images. The main difference between the NNs lies in the varying ranges of the five IOPs for which they are trained: pigment absorption (a_{pig}, m^{-1}), detritus (a_{det}, m^{-1}), gelbstoff (a_{gelb}, m^{-1}), scattering of white particles (b_{wit}, m^{-1}), and typical sediment scatter (b_{part}, m^{-1}) [23]. Additionally, unlike C2RCC and C2X, C2XC does not use b_{wit} or b_{part}, but rather the total backscattering (b_{tot}, m^{-1}) is applied for this processor [44] (Table 5).

Because of the different ranges used for training the NNs, C2RCC is preferably used for eutrophic to mesotrophic waters and the C2X is recommended for high concentrations of suspended material and chl-*a* concentrations, whereas C2XC is for complex water types. The main output of the algorithms is the directional water-leaving reflectance, which allows for the appropriate estimation of in-water constituents [23].

Table 5. Ranges of IOPs for training the NNs of C2RCC, C2X and C2XC, where a_{pig} is the pigment absorption, a_{det} is the absorption of detritus, a_{CDOM} is the colored dissolved organic matter, b_{wit} is the scattering of white particles, and b_{part} is the sediment scattering [23,44].

Processor	a_{pig} (m^{-1})	a_{det} (m^{-1})	a_{gelb} (m^{-1})	b_{wit} (m^{-1})	b_{part} (m^{-1})	b_{tot} (m^{-1})
C2RCC	~0–5.3	~0–5.9	~0–1	~0–60	~0–60	-
C2X	~0–51	~0–60	~0–60	~0–590	~0–590	-
C2XC	~0–30.81	~0–17	~0–4.25	-	-	~0–1000

The C2RCC-Nets are equipped with default parameters designed for quick image processing. The default values relevant to this study include salinity (35 PSU), water temperature (15 °C), air pressure at sea level (1000 hPa), ozone (330 DU), and elevation (0.0 m a.s.l). In this study, the default value for salinity was neglected (0.0001 PSU), while elevation was set according to the location of each lake (Table 1). Finally, water temperature data were available for each day and were used accordingly. The water temperatures applied in the image processing are detailed in the Supplementary Materials (Table S1). All other values were kept in default mode.

2.6. Quality and Uncertainty of C2RCC, C2X and C2XC

A mask composed of quality flags was used to filter out inaccurate data across the scenes, ensuring the retention of only valid pixels (Valid_PE) and the elimination of cloud interference (cloud_risk). Additionally, the uncertainty flag, defined as out-of-scope (OOS), can be raised due to anomalies in the spectral data or the water-leaving reflectances and IOPs. In particular, the OOS flag is raised when the data does not fall within the training range of the algorithm. In this study, uncertainties related to both the atmospheric (Rtosa_OOS) and the in-water (Rhow_OOS) components were applied. This step was employed to avoid potentially unreliable results, as the presence of these flags indicates that the transparency outputs might not accurately reflect the water's optical properties.

Once these steps were completed, the kd_z90max products, which refers to the K_d where 90% of the light has dissipated in the water column, were extracted (Equation (1)). At this depth, physical theory concerning the optical properties of waters states that SD aligns with the point where approximately 10% of the incident light remains available [7,45,46] (Equation (2)). This can be expressed as follows:

$$\text{kd\_z90max} = \frac{1}{kd\_min} \tag{2}$$

where *kd_min* is the signal depth at the wavelength with maximum transparency.

2.7. Spatial Filtering of Datasets

Prior to conducting statistical analysis, SD data points were integrated into the spatial analysis. To address spatial resolution and enhance the reliability of the satellite readings, the data were processed to work with 3 × 3 pixel windows centered at the in situ sampling locations. This approach ensured that each measurement represented the average of the surrounding nine pixels, thereby reducing noise and increasing the accuracy of the satellite-derived information [47]. To mitigate the potential for errors in satellite readings, a buffer zone of −200 m around the lake perimeters was established to exclude any data points that might be adversely affected by adjacency effects or the lake bottom reflectance [8]. Consequently, data points falling within this −200 m buffer were systematically discarded from the analysis, ensuring that only the most accurate and representative satellite data were used.

2.8. Statistical Analysis and Transparency Product Match-Ups

A correlation analysis was employed to evaluate the fit between the in situ SD data and the processed satellite-derived SD products. Because the data were not normally distributed,

Spearman's rank correlation, denoted as r_s, was utilized to understand the strength and direction of the data (Equation (3)). The statistical significance of the relationships was evaluated using *p*-values, which were interpreted within the bounds of a 95% confidence interval. Spearman's rank correlation can be expressed as follows:

$$r_s = 1 - \frac{6\sum_{i=1}^{n}(O_{ri} - E_{ri})^2}{n(n^2 - 1)} \quad (3)$$

where E_{ri} is the rank of the estimated value, O_{ri} is the rank of the observed value, and n is the number of observations.

The Root Mean Square Error (RMSE), Mean Absolute Error (MAE), and bias were also used for statistical analysis. The RMSE (4) measures the error of a model in predicting quantitative data, the MAE (5) is the measure of errors between paired observations expressing the same phenomenon, and bias (6) measures the systematic error that results when the average of the predictions made by the model differs from the actual average of the observed outcomes. RMSE, MAE, and bias were normalized by the mean (nRMSE, nMAE and nbias) to better understand these metrics. Therefore, the results are shown in SD units (m) and percentages (%). These three variables can be expressed as follows:

$$RMSE = \sqrt{\frac{1}{n}\sum_{i=1}^{n}(E_i - O_i)^2} \quad (4)$$

$$MAE = \frac{1}{n}\sum_{i=1}^{n}|E_i - O_i| \quad (5)$$

$$bias = \frac{1}{n}\sum_{i=1}^{n}(E_i - O_i) \quad (6)$$

where E_i is the estimated value, O_i is the observed value, and $\overline{O}$ is the mean value of O_i.

Finally, the Wilcoxon signed-rank test, a non-parametric alternative to the *t*-test, was used to determine significant differences between the results of the NNs for each lake [48].

3. Results

3.1. Inspection of the Dataset via Trophic State Index

The TSI was calculated using the compiled SD data to ensure that the lakes effectively represented different trophic states (Figure 2). Lake Lanalhue predominantly presents mesotrophic conditions, with TSI values mostly between 35 and 55, although several data points extend into the eutrophic range, reaching values close to TSI = 65. The TSI values for Lanalhue generally exceed those of Lake Villarrica, except for one data point where the TSI is 38, indicating mesotrophic conditions with occasional shifts towards eutrophic levels. In contrast, Lake Villarrica's TSI values mostly fall within the mesotrophic range, with nearly half of the data points bordering oligotrophic conditions. Overall, Villarrica features lower TSI values compared to Lanalhue. For Lake Panguipulli, the TSI values are predominantly within the oligotrophic range, with most values below 30, and only one data point bordering the mesotrophic range.

3.2. SD Match-Up in Eutrophic Lake Lanalhue

The images acquired for Lake Lanalhue did not raise any quality flags, which indicates that the input spectrum to the atmospheric correction (Rtosa) and the IOP retrieval networks (IoPneural) were within the training range. Similarly, Cloud_risk and Valid_PE did not indicate the presence of clouds nor invalid pixels. Following the methods applied in this study, the introduction of the 200 m buffer around the perimeter of the lake reduced the amount of available data to n = 27. Nonetheless, no images were eliminated for the correlation analysis. As a result, the data for Lake Lanalhue was comprised of data from 2018–2023.

Results show that satellite-derived SD using C2XC produced the strongest positive correlation, reaching r_s = 0.889 supported by a *p*-value < 0.05 (Figure 3). Similarly to C2XC, significant correlations (*p*-value < 0.05) with r_s values of 0.852 and 0.849 were achieved for C2RCC and C2X, respectively. The results show close agreement between lower transparencies approximately until 2.5 m, with a noticeable break towards overestimations beyond this point for C2RCC and C2XC. In contrast, C2X underestimated SD predictions in the lower SD ranges.

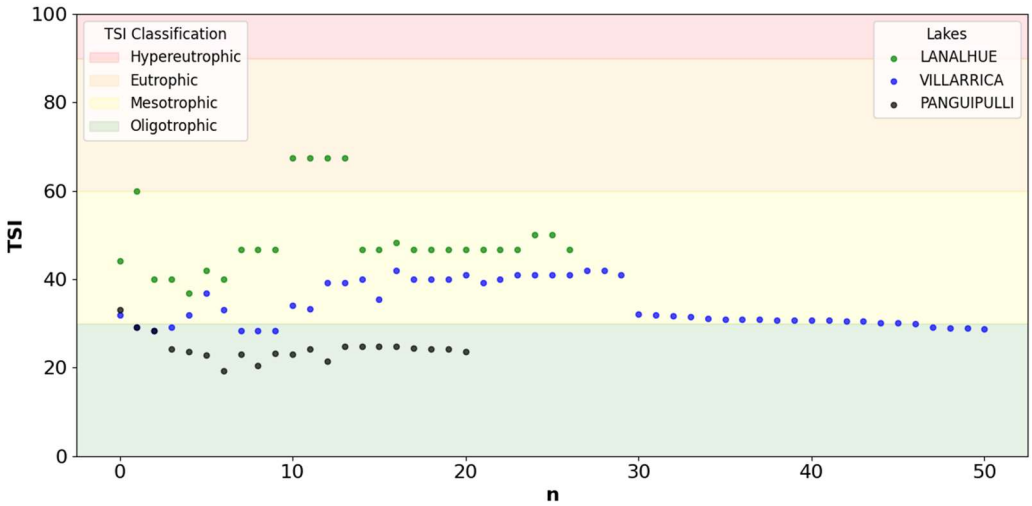

Figure 2. Validation dataset for Lakes Lanalhue (n = 27), Villarrica (n = 51), and Panguipulli (n = 21) categorized into hypereutrophic, eutrophic, mesotrophic, and oligotrophic ranges based on TSI calculations using SD.

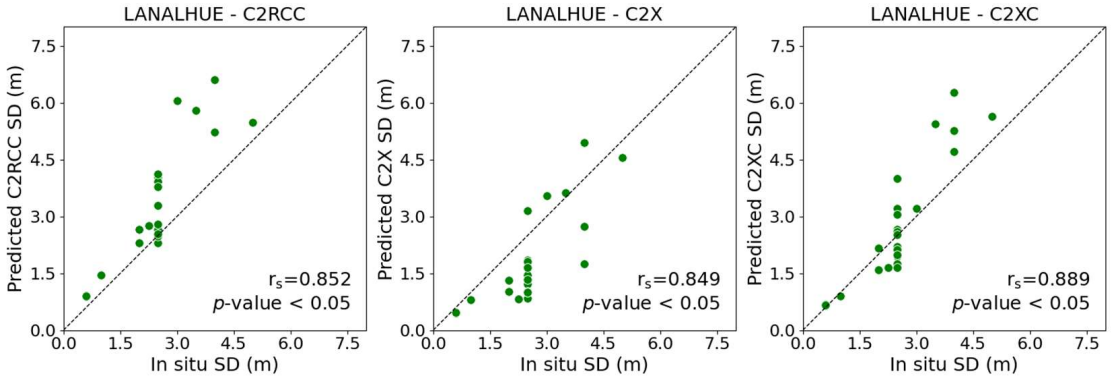

Figure 3. Correlation between the in situ SD and the satellite-derived SD using C2RCC, C2X and C2XC for Lake Lanalhue.

The precision assessment for Lake Lanalhue demonstrates the lowest nRMSE (33.13%) and nMAE (23.51%) for the C2XC, indicating superior fit to the in situ data compared to the other NNs. Although both C2RCC and C2X exhibit high correlation coefficients, their nRMSE and nMAE values are higher, reaching 56.88% and 43.35%, respectively, indicating a high divergence between predicted and true measurements. Additionally, the nbias indicates an overestimation of only 8.57% for the C2XC products, in contrast to 36.89% for C2RCC and an underestimation of −29.84% for C2X (Table 6). These biases suggest that while C2XC might be the preferred method for general SD estimation in this lake, adjustments or combined approaches might be necessary for accurate measurements across the full range of water clarity.

Table 6. Accuracy assessment of SD retrieval for Lake Lanalhue using C2RCC, C2X and C2XC.

Net	r_s	*p*-Value	RMSE (m)	nRMSE (%)	MAE (m)	nMAE (%)	bias (m)	nbias (%)
C2RCC	0.852	<0.05	1.383	56.88	0.913	37.53	0.897	36.89
C2X	0.849	<0.05	1.054	43.35	0.894	36.79	−0.725	−29.84
C2XC	0.889	<0.05	0.806	33.13	0.572	23.51	0.208	8.57

SD maps produced for Lake Lanalhue using C2RCC, C2X, and C2XC were accompanied by a Sentinel 2 MSI true color composite (RGB) using the red (665 nm), green (560 nm), and blue (490 nm) bands to inspect the results (Figure 4). The RGB images show distinct color changes across the years, particularly in the southeastern bay of the lake, which consistently exhibits lower transparency. This area is marked by sharper yellow tones in the SD maps, indicating shallow SD reaching approximately 0.5 m, suggesting higher concentrations of particulate matter or algae. In contrast, other regions of the lake, especially the central and northern parts, maintain clearer waters, with transparency levels typically ranging from around 7 to 4 m. Furthermore, these patterns are observed throughout the years, although recent imagery reveals an increase in yellow hues, suggesting a trend towards reduced water clarity over time. Nevertheless, differences between the NNs are apparent. The C2RCC NN shows darker blue tones, indicating depths > 10 m, especially concentrated along the lake's margins and bay areas. Additionally, it displays darker color values for depths ranging from approximately 7 to 4 m in other parts of the lake. In contrast to C2RCC, the C2X and C2XC images display consistent mid-range transparency around 4.0 m throughout the central parts of the lake for the dates 13 February 2018 and 18 January 2022, while showing lower values ($\leq$4 m) for C2X by 22 February 2023.

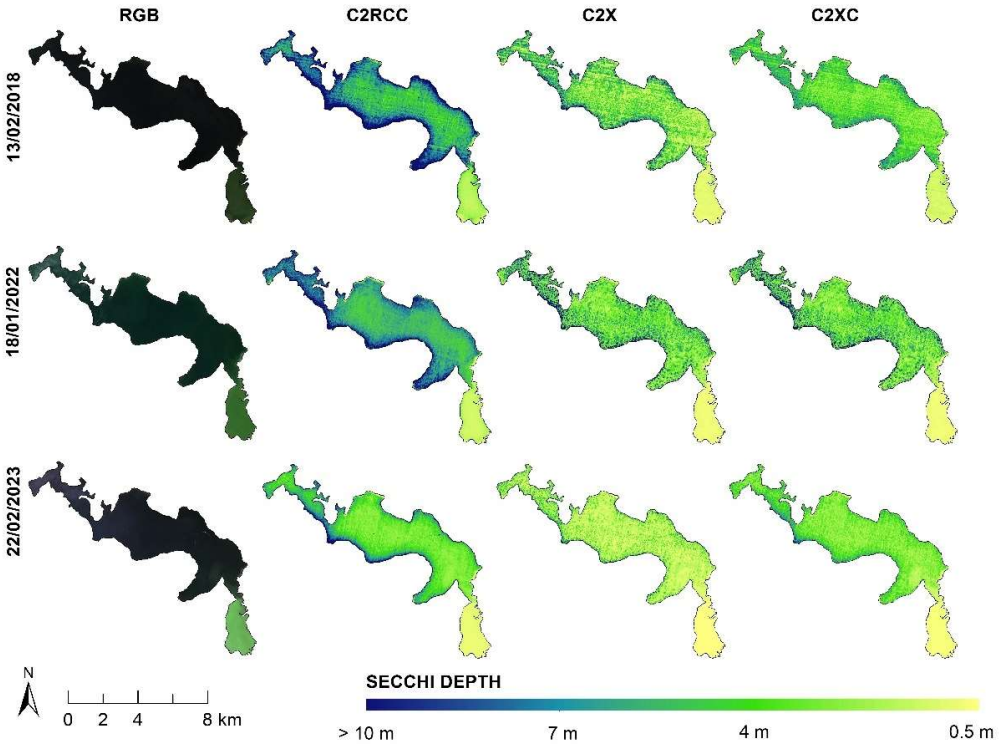

Figure 4. Multitemporal maps of SD retrieval using C2RCC, C2X and C2XC in Lake Lanalhue.

3.3. SD Match-Up in Oligo-Mesotrophic Lake Villarrica

In the case of Lake Villarrica, the analysis produced uncertainty flags on four of the eight dates (25 February 2019, 9 February 2021, 1 March 2021, and 13 January 2023). Along

with these masked out areas and the application of the 200 m buffer, a total of n = 51 were available for correlation analysis.

The results were less accurate in comparison with Lanalhue, where SD obtained by the C2RCC displayed the most robust correlation (r_s = 0.739). This indicates a robust positive relationship between predicted and in situ values, confirmed by a statistical significance of *p*-value < 0.05. Furthermore, predictions covered the entire range of observed values. However, the model shows tendencies of overestimation, reaching values approximately between 5 and 15 m—a much wider range (10 m) in comparison with the in situ dataset, which falls between 3.5 and 11 m (Table 2). The tendency of overestimation is particularly pronounced at higher SD values, reaching 4 m above the observed values.

C2X showed a significant (*p*-value < 0.05) but weaker correlation (r_s = 0.492) and a greater dispersion of datapoints in comparison to C2RCC. Overall, C2X predictions were generally lower (approximately between 2 and 10 m) with a notable underestimation, particularly at higher values. In this case, the predictions were concentrated towards the lower ends of the SD range, surpassing observed values.

C2XC achieved a moderate correlation with r_s = 0.618, which was also statistically significant (*p*-value < 0.05). The performance of C2XC was superior to C2X, and demonstrated a closer alignment with in situ values, which ranged approximately between 4 and 10 m. Although this NN demonstrates a slight overestimation, it maintains a better consistency across the SD range compared to C2RCC and C2X (Figure 5).

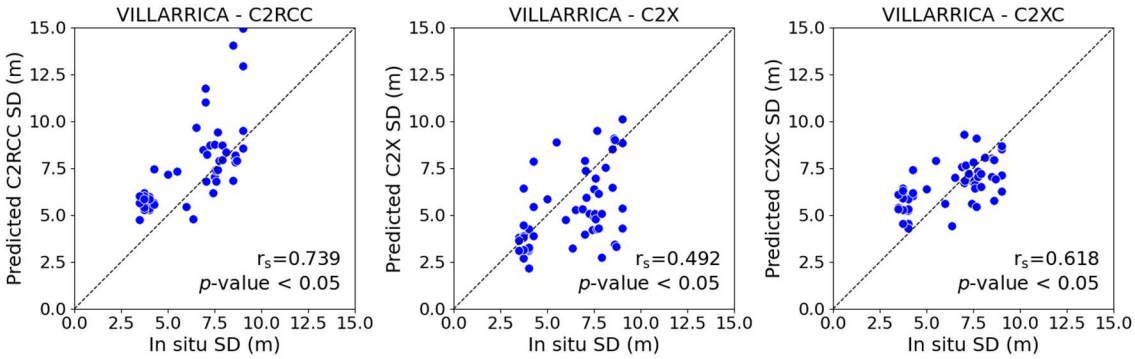

Figure 5. Correlation between the in situ SD and the satellite-derived SD using C2RCC, C2X and C2XC for Lake Villarrica.

Although the C2RCC NN exhibits the highest correlation for Lake Villarrica, it presents nRMSE (32.98%) and nMAE (25.36%) values indicating less precise estimations (Table 7). This shows that while C2RCC predictions achieve an overall trend, SD values tend to diverge from the actual measurements, causing uncertainty in the predictions. This divergence is particularly evident in the model's tendency to overestimate SD, with a positive nbias of 19.27%. The systematic overestimation of SD predictions using the C2RCC NN would suggest higher transparencies, potentially leading to classification errors that could impact the assessment of the lake.

Table 7. Accuracy assessment of SD retrieval for Lake Villarrica using C2RCC, C2X and C2XC.

Net	r_s	*p*-Value	RMSE (m)	nRMSE (%)	MAE (m)	nMAE (%)	bias (m)	nbias (%)
C2RCC	0.739	<0.05	2.100	32.98	1.614	25.36	1.227	19.27
C2X	0.49	<0.05	2.284	35.87	1.755	27.56	−1.024	−16.08
C2XC	0.618	<0.05	1.571	24.67	1.3216	20.67	0.268	4.21

Conversely, the C2X NN records the highest nRMSE (35.87%) and nMAE (27.56%), reflecting the least precise estimations among the NNs. The negative nbias of −16.08%

significantly highlights the C2X's tendency to underestimate SD, which might result in conservative evaluations of transparency, potentially leading to overestimations of ecological or pollution problems occurring in Lake Villarrica.

The C2XC NN, offering the lowest nRMSE (24.67%) and nMAE (20.67%), provides the most accurate and precise depth estimations among the processors for this lake. The minor nbias of 4.21% with C2XC indicates a slight overestimation but is closer to true measurements.

Following the mapping of Lake Villarrica, the C2RCC SD products present a broader range of SDs, as seen from the darker blue hues (Figure 6). Notably, on 25 February 2019 and 1 March 2021, darker blues indicate higher transparencies >15 m, showing indications of failure in the NNs, where maximum in situ SD values reach 11 m. This anomaly is also evident in the bay areas of the lake, where greater inputs from land occur, making these waters more complex. In comparison, the C2X NN produces images where higher transparency values are less pronounced, but are still present in the form of noise across all images. Nonetheless, the results of the C2X NN align better with the in situ dataset. Furthermore, this NN vividly captures changes in transparency due to bloom formations reaching values as low as 0.5 m, as seen in the brighter yellow regions in the northwestern part of the lake on 2 February 2023 and 23 January 2024. The C2XC results, while showing similar patterns to C2X in terms of transparency during bloom events, tend to feature even more distinct bright colors in the presence of blooms, reinforcing its sensitivity to high particulate content in the water.

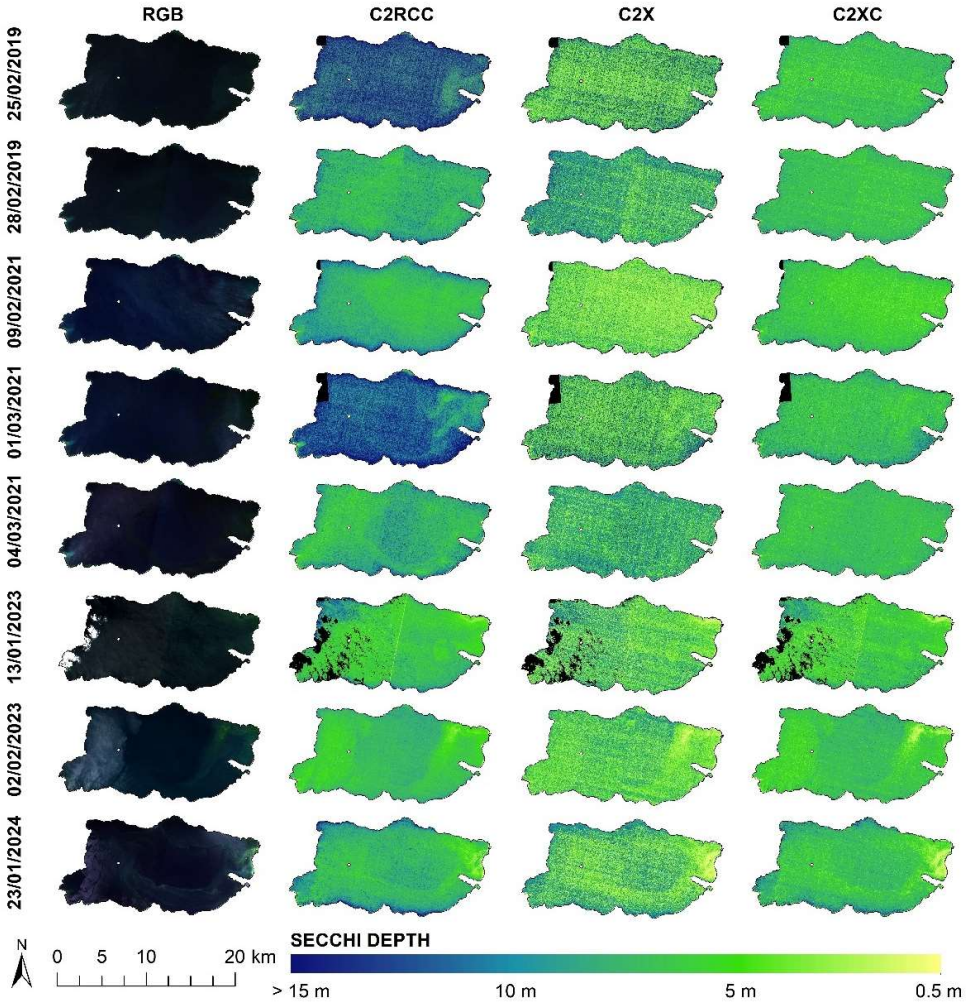

Figure 6. Multitemporal maps of Secchi depth retrieval using C2RCC, C2X and C2XC in Lake Villarrica.

3.4. SD Match-Up for Ultra-Oligotrophic Lake Panguipulli

Flags for Lake Panguipulli were raised on three of the six images, corresponding to 31 January 2019, 24 February 2021, and 18 January 2023. After keeping the most accurate and representative satellite data for correlation analysis (n = 21), the results for this lake demonstrated the overall weakest results. C2RCC retained the highest positive correlation of 0.533, with statistical significance (p-value = 0.05). In contrast, both C2X and C2XC showed negative, non-significant correlations of −0.313 and −0.408, respectively (Figure 7).

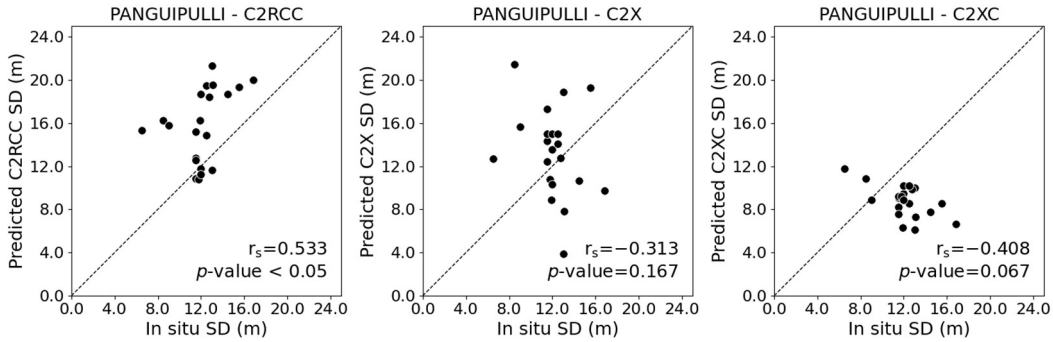

Figure 7. Correlation between the in situ SD and the satellite-derived SD using C2RCC, C2X and C2XC for Lake Panguipulli.

SD estimations for Lake Panguipulli showed unfavorable results compared to Lakes Lanalhue and Villarrica, highlighting the need for careful consideration when applying these models to lakes with lower trophic states. The C2RCC, while having a positive correlation coefficient, presents very high nRMSE (40.67%) and nMAE (33.64%) values, suggesting significant discrepancies between the estimated and actual SD. The large positive nbias of 30.51% indicates substantial overestimation (Table 8). The C2X and C2XC NNs exhibit negative correlation coefficients, with values of r_s = −0.313 and r_s = −0.408, respectively. This inverse relationship between the measured and satellite-derived SD reveals errors, exposing inadequate performances and a fundamentally incorrect relationship, which is inconsistent with the expected outcomes.

Table 8. Accuracy assessment of SD for Lake Panguipulli using C2RCC, C2X and C2XC.

Net	r_s	p-Value	RMSE (m)	RMSE (%)	MAE (m)	MAE (%)	bias (m)	nbias (%)
C2RCC	0.533	0.013	4.908	40.67	4.060	33.64	3.682	30.51
C2X	−0.313	0.167	5.178	42.90	4.203	34.82	1.248	10.34
C2XC	−0.408	0.067	4.596	38.08	3.995	33.10	−3.265	−27.05

3.5. Evaluation of the Significance Differences Between NNs

The Wilcoxon signed-rank test revealed that all NNs were significantly different ($p < 0.05$ in terms of estimating SD (Table 9).

The most pronounced difference was found in the comparison between C2RCC and C2X in Lake Lanalhue. Here, all instances fell within the positive rank (n = 27), showing a clear divergence in SD estimations. Similar results were found for C2RCC when compared to C2XC, where very high values (n = 25) were an indication of the differences between the NNs, while C2X vs. C2XC had only one instance of falling into the positive rank.

Similar results were found for Lake Villarrica, where overall results again confirm that the NNs differ significantly in their performance (p-value < 0.05). The pattern is also similar in how the Wilcoxon signed-rank test delivers the results of this lake in comparison to the results in Lake Lanalhue. Here, C2RCC consistently produces higher estimations, while C2X produces lower values in comparison to C2XC. The results, however, show that a lower percent in positive ranks is achieved for C2RCC (82.4%) in comparison to C2X

and C2XC in Lake Lanalhue, which reach 100% and 92.6%, respectively. The same occurs with C2X, which only reaches 3.70% in Lake Lanalhue and increments to 21.60% in Lake Villarrica. This shows that the NNs consistently produce values that fall in the order C2RCC > C2XC > C2X, which is coherent with the bias of all NNs in Lanalhue and Villarrica.

Table 9. Wilcoxon signed-rank test for C2RCC, C2X, and C2XC for Lake Lanalhue and Villarrica.

Lake	Comparison	Positive Ranks			Negative Ranks			Z-Score	*p*-Value
		n	Mean	Sum	n	Mean	Sum		
Lanalhue	C2RCC vs. C2X	27	14	378	0	0	0	−4.54	<0.05
	C2RCC vs. C2XC	25	15	373	2	2	5	−4.24	<0.05
	C2X vs. C2XC	1	8	8	26	15	370	15.00	<0.05
Villarrica	C2RCC vs. C2X	42	29	1251	9	8	75	−4.71	<0.05
	C2RCC vs. C2XC	40	28	1140	11	17	186	−3.01	<0.05
	C2X vs. C2XC	11	10	110	40	30	1216	6.85	<0.05

4. Discussion

4.1. Selection of the Correct NNs

In our study, C2XC provided superior results for both Lake Lanalhue and Lake Villarrica in estimating SD, highlighting the importance of the NNs' original design and their IOPs ranges. First, both C2RCC and C2X were originally developed for coastal waters [23], suggesting that the optical signatures found in our lakes may be challenging for these NNs. In contrast, C2XC was specifically designed for darker inland waters [44], potentially making it more suitable for the lakes in our study. Furthermore, a_{pig} for C2X (0–51 m^{-1}) is wider than that of C2XC (0–30.81 m^{-1}), which initially seems counterintuitive to C2XC's superior performance (Table 5). However, this suggests that the NNs are not solely determined by having the widest possible ranges; instead, the advantage likely stems from intermediate ranges across its IOPs, including a_{det} and a_{gelb}. This is also supported by the nbias introduced in C2RCC and C2X in our results for Lake Lanalhue and Villarrica, where the narrower ranges of C2RCC cause overfitting, while the wider ranges of C2X consistently cause underfitting (Tables 6 and 7). Thus, the width of IOP ranges may deviate from the actual solution of the inversion to IOPs, resulting in potentially less precise retrievals [49,50].

The b_{tot} also offers an understanding of the consistency of C2XC's superiority in waters with higher trophic states. In comparison to C2RCC and C2X, which use b_{wit} and b_{part} individually in their NNs, C2XC uses total scattering, an integrated approach. Since b_{tot} measures how particles affect light scattering in the water column, factors like sediments and/or blooms in eutrophic lakes might contribute to the complexity of the studied lakes. The wider range of b_{tot} (0–1000 m^{-1}) introduced in the C2XC NN seems to be particularly favorable for SD values below 2.5 m (Figure 4). Our findings align with other studies that have found C2XC to be superior in estimating SD. For example, [51] reported better performance (r = 0.97) with C2XC when comparing kd_z90max products in the Ecuadorian high Andean Lake Colta. These results are particularly relevant as in situ data for this lake ranged from values between 1.50 and 2.70 m, which further supports the observed 2.50 m threshold in our results. Similarly, a study from Spain by [50] achieved better correlations with C2XC (r = 0.94) compared to C2RCC (r = 0.77) and C2X (r = 0.82), using an SD range (0.45–7.7 m), like our dataset for Lake Lanalhue. On the contrary, [52], who used LaSRC, developed a global SD model for Canadian lakes, report that the model only worked for SD values > 1 m, often resulting in overpredictions in eutrophic lakes. Given these

results, this suggests that different lakes require different atmospheric corrections—or, in our case, NNs—based on their OWT or thresholds that can be related to trophic state. These results also highlight the importance of having in situ IOPs data for a better understanding of the optical properties within the water column and for future local tuning of remote sensing algorithms. This is particularly important in cases where both inter- and intra-lake variations occur, as observed in Lanalhue and Villarrica (Figures 4 and 6). This necessity is further supported by the Wilcoxon signed-rank test conducted in our study, which confirms that each NN produces significantly different results (Table 9).

4.2. C2RCC-NNs and Lakes with Low Trophic Index

Our findings reveal that SD estimations show stronger correlations in eutrophic inland waters, with declining performance in lakes of lower trophic states. This pattern is evident across the studied lakes, in the order Lanalhue (eutrophic), Villarrica (oligo-mesotrophic), and Panguipulli (oligotrophic).

The inferior tendencies in lower trophic levels suggest an underrepresentation of OWTs (and consequently IOPs) within the datasets used for training the NNs. Studies have already noted scarce data availability for clear, very clear, sediment-laden and CDOM-rich waters [53,54]. These datasets also contain a low representativeness of lakes in the Southern Hemisphere, which are predominantly confined to Brazil and South Africa [42,55]. Therefore, bias might be introduced into validation, favoring certain OWTs [2]. Furthermore, an intercomparison study of atmospheric correction processors across different OWTs has shown that certain processors produce better outcomes depending on the OWTs. This study also expands upon the utility of atmospheric correction processors over different spectral bands, indicating that iCOR performs better in the 443 nm band in comparison to other processors, while C2X performs better in the red band (664 nm) [24]. Similar results were observed by [25] in several German lakes; however, this study found ACOLITE to perform better in the 443 nm band. This study also found that the performance of C2RCC improved when only considering meso- to eutrophic lakes. These findings underscore the importance of validating atmospheric correction methods, which apply not only to different OWTs or trophic states but also to the specific parameter that is being estimated. Therefore, an integrated approach that combines the strengths of various processors (or NNs in this case) might be more suitable for improving overall water quality estimations.

In response to these challenges, recent efforts have been made to compile more comprehensive global SD datasets, as seen in the works of [56] and [57]. Although these datasets still have limited representation of waters with low trophic states, they mark a significant step toward better global representation. Notably, newer approaches, such as the study by [58], have demonstrated promising results in clearer inland waters. Using a Random Forest algorithm, this study achieved an r = 0.74 and RMSE = 0.72 m. Despite utilizing a relatively small dataset (n = 125 measurements) for training and validation, the study showcases the potential of applying advanced algorithms even with limited data, including in low productivity lakes.

5. Conclusions

This study demonstrated the potential of the C2RCC-NNs to derive SD measurements in lakes with different trophic states. Our results show that C2XC outperforms in higher trophic levels, while challenges persist in accurately assessing lower trophic state categories. The intermediate IOP ranges in C2XC, and the use of b_{tot}, are particularly useful for SDs thresholds <2.5 m. This underscores the need for model-specific calibration of C2RCC-NNs, as lakes with different OWTs and trophic states may require tailored IOP training ranges for optimal performance.

Our results show that satellite imagery has the potential to significantly expand the scope of environmental monitoring of Chilean inland waters, and that this could be improved with more in situ understanding of the optical properties (apparent and inherent) of the water column. The use of these freely available products offers a valuable opportunity

to monitor changes in lakes over time, suggesting that incorporating these techniques into national water management strategies could enhance the detection and management of water quality trends.

Further research should focus on identifying appropriate thresholds and developing an integrated NN approach to improve the accuracy and reliability of water quality estimations. Additionally, refining remote sensing methods and expanding monitoring coverage of IOPs is essential in underrepresented areas, particularly in the Global South. This could enhance current validation processes and, consequently, global models. Lastly, newly available SD datasets, in conjunction with machine learning algorithms, also offer promising solutions to improve existing models.

Supplementary Materials: The following supporting information can be downloaded at: https://www.mdpi.com/article/10.3390/rs16224327/s1, Table S1: C2RCC, C2X and C2XC processing parameters for lake Lanalhue, Villarica and Panguipulli.

Author Contributions: Conceptualization, D.R.-R. and I.O.; methodology, D.R.-R. and I.O.; software, D.R.-R.; validation, D.R.-R. and C.E.; formal analysis, D.R.-R.; investigation, D.R.-R.; resources, J.L.A.; data curation, D.R.-R., M.P.-M., M.L.-S. and C.E.; writing—original draft preparation, D.R.-R.; writing—review and editing, D.R.-R., J.L.A., I.O., C.E., M.L.-S. and R.U.; visualization, D.R.-R.; supervision, J.L.A., I.O. and M.L.-S.; project administration, D.R.-R. and P.A.-Á.; funding acquisition, J.L.A. All authors have read and agreed to the published version of the manuscript.

Funding: This research was funded by the Beca de Doctorado Nacional de la Agencia de Investigación y Desarrollo ANID/21201043 and the APC was funded by CRHIAM Water Center, Project ANID/FONDAP/15130015 and ANID/FONDAP/1523A0001.

Data Availability Statement: Satellite data are freely available from the Copernicus Open Access Hub (https://browser.dataspace.copernicus.eu/) and the Sentinel Application Platform (http://step.esa.int/main/toolboxes/snap/). In situ water quality data from secondary sources can be downloaded from the Dirección General de Aguas (DGA: http://www.dga.cl/), and the Sistema Nacional de Información Ambiental (SINIA: https://sinia.mma.gob.cl/).

Acknowledgments: We want to thank CRHIAM Water Center, Project ANID/FONDAP/15130015 and ANID/FONDAP/1523A0001 and acknowledge Claudia Leal, Herman Benavides and Pablo Millar for supporting field campaigns and laboratory analysis, Los Vigilantes del Lago, for their support during field campaigns, as well as the projects ANILLO ATE220060, Fondecyt Regular 1231551 and Fondecyt Regular 1240447, Instituto Iberoamericano de Desarrollo Sostenible (IIDS), Universidad Autónoma de Chile.

Conflicts of Interest: The authors declare no conflicts of interest.

References

1. Ogashawara, I.; Mishra, D.R.; Gitelson, A.A. Chapter 1—Remote Sensing of Inland Waters: Background and Current State-of-the-Art. In *Bio-Optical Modeling and Remote Sensing of Inland Waters*; Mishra, D.R., Ogashawara, I., Gitelson, A.A., Eds.; Elsevier: Amsterdam, The Netherlands, 2017; pp. 1–24.
2. Palmer, S.C.J.; Kutser, T.; Hunter, P.D. Remote sensing of inland waters: Challenges, progress and future directions. *Remote Sens. Environ.* **2015**, *157*, 1–8. [CrossRef]
3. Gholizadeh, M.H.; Melesse, A.M.; Reddi, L. A Comprehensive Review on Water Quality Parameters Estimation Using Remote Sensing Techniques. *Sensors* **2016**, *16*, 1298. [CrossRef] [PubMed]
4. Topp, S.N.; Pavelsky, T.M.; Jensen, D.; Simard, M.; Ross, M.R.V. Research Trends in the Use of Remote Sensing for Inland Water Quality Science: Moving Towards Multidisciplinary Applications. *Water* **2020**, *12*, 169. [CrossRef]
5. Zielinski, O. The History and Future of the Secchi Disk. In *Angelo Secchi and Nineteenth Century Science: The Multidisciplinary Contributions of a Pioneer and Innovator*; Chinnici, I., Consolmagno, G., Eds.; Springer International Publishing: Cham, Switzerland, 2021; pp. 215–224.
6. Dodds, W.K.; Whiles, M.R. Chapter 3—Movement of Light, Heat, and Chemicals in Water. In *Freshwater Ecology*, 2nd ed.; Dodds, W.K., Whiles, M.R., Eds.; Academic Press: London, UK, 2010; pp. 45–64.
7. Kirk, J.T. *Light and Photosynthesis in Aquatic Ecosystems*; Cambridge University Press: Cambridge, UK, 1994.
8. Zhang, Y.; Zhang, Y.; Shi, K.; Zhou, Y.; Li, N. Remote sensing estimation of water clarity for various lakes in China. *Water Res.* **2021**, *192*, 116844. [CrossRef]

9. Secchi, P.A. Relazione delle esperienze fatte a bordo della pontificia pirocorvetta Imacolata Concezione per determinare la trasparenza del mare. *Il Nuovo Cimento* **1864**, *20*, 205–238.
10. Lee, Z.; Shang, S.; Hu, C.; Du, K.; Weidemann, A.; Hou, W.; Lin, J.; Lin, G. Secchi disk depth: A new theory and mechanistic model for underwater visibility. *Remote Sens. Environ.* **2015**, *169*, 139–149. [CrossRef]
11. Benavides, G. *Redefinición de la Red Mínima de Lagos*; Dirección General de Aguas Santiago: Santiago, Chile, 2009.
12. Huovinen, P.; Ramírez, J.; Caputo, L.; Gómez, I. Mapping of spatial and temporal variation of water characteristics through satellite remote sensing in Lake Panguipulli, Chile. *Sci. Total Environ.* **2019**, *679*, 196–208. [CrossRef]
13. Rodríguez-López, L.; Alvarez, D.; Bustos Usta, D.; Duran-Llacer, I.; Bravo Alvarez, L.; Fagel, N.; Bourrel, L.; Frappart, F.; Urrutia, R. Chlorophyll-a Detection Algorithms at Different Depths Using In Situ, Meteorological, and Remote Sensing Data in a Chilean Lake. *Remote Sens.* **2024**, *16*, 647. [CrossRef]
14. Rodríguez-López, L.; Duran-Llacer, I.; Bravo Alvarez, L.; Lami, A.; Urrutia, R. Recovery of Water Quality and Detection of Algal Blooms in Lake Villarrica through Landsat Satellite Images and Monitoring Data. *Remote Sens.* **2023**, *15*, 1929. [CrossRef]
15. Rodríguez-López, L.; Duran-Llacer, I.; González-Rodríguez, L.; Abarca-del-Rio, R.; Cárdenas, R.; Parra, O.; Martínez-Retureta, R.; Urrutia, R. Spectral analysis using LANDSAT images to monitor the chlorophyll-a concentration in Lake Laja in Chile. *Ecol. Inform.* **2020**, *60*, 101183. [CrossRef]
16. Rodríguez-López, L.; González-Rodríguez, L.; Duran-Llacer, I.; Cardenas, R.; Urrutia, R. Spatio-temporal analysis of chlorophyll in six Araucanian lakes of Central-South Chile from Landsat imagery. *Ecol. Inform.* **2021**, *65*, 101431. [CrossRef]
17. Yépez, S.; Velásquez, G.; Torres, D.; Saavedra-Passache, R.; Pincheira, M.; Cid, H.; Rodríguez-López, L.; Contreras, A.; Frappart, F.; Cristóbal, J.; et al. Spatiotemporal Variations in Biophysical Water Quality Parameters: An Integrated In Situ and Remote Sensing Analysis of an Urban Lake in Chile. *Remote Sens.* **2024**, *16*, 427. [CrossRef]
18. Barraza-Moraga, F.; Alcayaga, H.; Pizarro, A.; Félez-Bernal, J.; Urrutia, R. Estimation of Chlorophyll-a Concentrations in Lanalhue Lake Using Sentinel-2 MSI Satellite Images. *Remote Sens.* **2022**, *14*, 5647. [CrossRef]
19. Rodríguez-López, L.; Duran-Llacer, I.; González-Rodríguez, L.; Cardenas, R.; Urrutia, R. Retrieving Water Turbidity in Araucanian Lakes (South-Central Chile) Based on Multispectral Landsat Imagery. *Remote Sens.* **2021**, *13*, 3133. [CrossRef]
20. Vanhellemont, Q. Adaptation of the dark spectrum fitting atmospheric correction for aquatic applications of the Landsat and Sentinel-2 archives. *Remote Sens. Environ.* **2019**, *225*, 175–192. [CrossRef]
21. De Keukelaere, L.; Sterckx, S.; Adriaensen, S.; Knaeps, E.; Reusen, I.; Giardino, C.; Bresciani, M.; Hunter, P.; Neil, C.; Van der Zande, D. Atmospheric correction of Landsat-8/OLI and Sentinel-2/MSI data using iCOR algorithm: Validation for coastal and inland waters. *Eur. J. Remote Sens.* **2018**, *51*, 525–542. [CrossRef]
22. Sayler, K.; Zanter, K. *Landsat 8 Collection 2 (C2) Level 2 Science Product (L2SP) Guide LSDS-1619*; Version 2.0; EROS Sioux Falls: South Dakota, SD, USA, 2021.
23. Brockmann, C.; Doerffer, R.; Peters, M.; Kerstin, S.; Embacher, S.; Ruescas, A. Evolution of the C2RCC neural network for Sentinel 2 and 3 for the retrieval of ocean colour products in normal and extreme optically complex waters. In Proceedings of the Living Planet Symposium, Prague, Czech Republic, 9–13 May 2016; p. 54.
24. Pahlevan, N.; Mangin, A.; Balasubramanian, S.V.; Smith, B.; Alikas, K.; Arai, K.; Barbosa, C.; Bélanger, S.; Binding, C.; Bresciani, M. ACIX-Aqua: A global assessment of atmospheric correction methods for Landsat-8 and Sentinel-2 over lakes, rivers, and coastal waters. *Remote Sens. Environ.* **2021**, *258*, 112366. [CrossRef]
25. Ogashawara, I.; Kiel, C.; Jechow, A.; Kohnert, K.; Ruhtz, T.; Grossart, H.-P.; Hölker, F.; Nejstgaard, J.C.; Berger, S.A.; Wollrab, S. The Use of Sentinel-2 for Chlorophyll-a Spatial Dynamics Assessment: A Comparative Study on Different Lakes in Northern Germany. *Remote Sens.* **2021**, *13*, 1542. [CrossRef]
26. Ogashawara, I.; Jechow, A.; Kiel, C.; Kohnert, K.; Berger, S.A.; Wollrab, S. Performance of the Landsat 8 Provisional Aquatic Reflectance Product for Inland Waters. *Remote Sens.* **2020**, *12*, 2410. [CrossRef]
27. Parra, O.; Valdovinos, C.; Urrutia, R.; Cisternas, M.; Habit, E.; Mardones, M. Caracterización y tendencias tróficas de cinco lagos costeros de Chile Central. *Limnetica* **2003**, *22*, 51–83. [CrossRef]
28. Centro EULA, Universidad de Concepción. *Estudio Limnológico para Sustentar Anteproyecto de la Norma Secundaria de Calidad Ambiental (NSCA) del Lago Lanalhue, Provincia de Arauco, Región del Biobío*; Licitación Pública: ID 608897-30-LQ18; Ministerio de Medio Ambiente: Concepción, Chile, 2020.
29. Secretaría Regional Ministerial del Medio Ambiente, Región de la Araucanía. *Informe Técnico de Antecedentes para Declarar a la Cuenca del Lago Villarrica Como Zona Saturada por Clorofila-"a", Transparencia y Fósforo Disuelto*; Departamento de Conservación de Ecosistemas Acuáticos, División de Recursos Naturales y Biodiversidad del Ministerio de Medio Ambiente: La Araucanía, Chile, 2017.
30. Aguayo, M.; Pauchard, A.; Azócar, G.; Parra, O. Cambio del uso del suelo en el centro sur de Chile a fines del siglo XX: Entendiendo la dinámica espacial y temporal del paisaje. *Rev. Chil. Hist. Nat.* **2009**, *82*, 361–374. [CrossRef]
31. Pizarro, J.; Vergara, P.M.; Cerda, S.; Briones, D. Cooling and eutrophication of southern Chilean lakes. *Sci. Total Environ.* **2016**, *541*, 683–691. [CrossRef] [PubMed]
32. Nimptsch, J.; Woelfl, S.; Osorio, S.; Valenzuela, J.; Moreira, C.; Ramos, V.; Castelo-Branco, R.; Leão, P.N.; Vasconcelos, V. First record of toxins associated with cyanobacterial blooms in oligotrophic North Patagonian lakes of Chile—A genomic approach. *Int. Rev. Hydrobiol.* **2016**, *101*, 57–68. [CrossRef]
33. Almanza, V.; Pedreros, P.; Dail Laughinghouse, H.; Félez, J.; Parra, O.; Azócar, M.; Urrutia, R. Association between trophic state, watershed use, and blooms of cyanobacteria in south-central Chile. *Limnologica* **2019**, *75*, 30–41. [CrossRef]

34. Campos, H.; Arenas, J.; Steffen, W.; Agüero, G. Morphometrical, physical and chemical limnology of Lake Panguipulli (Valdivia, Chile). *Neues Jahrb. Für Geol. Und Paläontologie Monatshefte* **1981**, *10*, 603–625. [CrossRef]
35. Alvial Chandía, I.E.; Dirección General de Aguas; Ingeniería y Gestión Ambiental Enlaces SPA. Evaluación de la Condición Trófica en Cuerpos Lacustres; DGA, Departamento de Conservación y Protección de los Recursos Hídricos. 2018. Available online: https://bibliotecadigital.ciren.cl/items/6e146774-36cb-4a12-8f20-52b931810e5b (accessed on 14 March 2024).
36. Juri, G.; Dirección General de Aguas. *Materia: Análisis de la Relación Entre Clorofila "a" y la Transparencia de los Lagos Monitoreados por la Red de Calidad de la DGA, y Elaboración de un Ranking de Lagos Basado en el Estado Trófico Otorgado por Estos Parámetros*; Dirección General de Aguas, Minuta DCPRH N°10: Santiago, Chile, 2018.
37. Centro Eula. *Monitoreo Limnológico de Áreas de Vigilancia Propuestas para una Futura Norma Secundaria de Calidad Ambiental (NSCA) en el Lago Lanalhue, Provincia de Arauco, Región del BioBío*; Ministerio de Medio Ambiente: Concepción, Chile, 2022.
38. Ministerio de Medio Ambiente. *Sexto Informe Nacional de Biodiversidad de Chile ante el Convenio Sobre la Diversidad Biológica (CDB)*; Ministerio de Medio Ambiente: Santiago, Chile, 2019.
39. Centro EULA. *Recopilación, Sistematización y Análisis de Información Disponible para la Elaboración de Normas Secundarias de Calidad Ambiental para la Protección de las Aguas de los Lagos Nor-Patagónicos de Chile*; Dirección General de Aguas: Concepción, Chile, 2021.
40. Carlson, R.E. A trophic state index for lakes. *Limnol. Oceanogr.* **1977**, *22*, 361–369. [CrossRef]
41. Zuhlke, M.; Fomferra, N.; Brockmann, C.; Peters, M.; Veci, L.; Malik, J.; Regner, P. SNAP (sentinel application platform) and the ESA sentinel 3 toolbox. In Proceedings of the Sentinel-3 for Science Workshop, Venice, Italy, 2–5 June 2015; p. 21.
42. Werdell, P.J.; Bailey, S.W. An improved in-situ bio-optical data set for ocean color algorithm development and satellite data product validation. *Remote Sens. Environ.* **2005**, *98*, 122–140. [CrossRef]
43. Nechad, B.; Ruddick, K.; Schroeder, T.; Oubelkheir, K.; Blondeau-Patissier, D.; Cherukuru, N.; Brando, V.; Dekker, A.; Clementson, L.; Banks, A.C.; et al. CoastColour Round Robin data sets: A database to evaluate the performance of algorithms for the retrieval of water quality parameters in coastal waters. *Earth Syst. Sci. Data* **2015**, *7*, 319–348. [CrossRef]
44. Ruescas, A. C2X-Complex. Available online: https://forum.step.esa.int/t/c2x-complex/29392 (accessed on 12 June 2023).
45. Preisendorfer, R.W. Secchi disk science: Visual optics of natural waters 1. *Limnol. Oceanogr.* **1986**, *31*, 909–926. [CrossRef]
46. Doerffer, R.; Goryl, P.; Brockmann, C.; Bourg, L. Algorithm Theoretical Bases Document (ATBD) for L2 processing of MERIS data of case 2 waters, 4 th reprocessing. *Rapp. Tech.* **2015**, *2*, 3–20.
47. Llodrà-Llabrés, J.; Martínez-López, J.; Postma, T.; Pérez-Martínez, C.; Alcaraz-Segura, D. Retrieving water chlorophyll-a concentration in inland waters from Sentinel-2 imagery: Review of operability, performance and ways forward. *Int. J. Appl. Earth Obs. Geoinf.* **2023**, *125*, 103605. [CrossRef]
48. Wilcoxon, F. Individual comparisons by ranking methods. *Biom. Bull.* **1945**, *1*, 80–83. [CrossRef]
49. Niroumand-Jadidi, M.; Bovolo, F.; Bruzzone, L.; Gege, P. Inter-Comparison of Methods for Chlorophyll-a Retrieval: Sentinel-2 Time-Series Analysis in Italian Lakes. *Remote Sens.* **2021**, *13*, 2381. [CrossRef]
50. Soriano-González, J.; Urrego, E.P.; Sòria-Perpinyà, X.; Angelats, E.; Alcaraz, C.; Delegido, J.; Ruíz-Verdú, A.; Tenjo, C.; Vicente, E.; Moreno, J. Towards the Combination of C2RCC Processors for Improving Water Quality Retrieval in Inland and Coastal Areas. *Remote Sens.* **2022**, *14*, 1124. [CrossRef]
51. Ayala Izurieta, J.E.; Beltrán Dávalos, A.A.; Jara Santillán, C.A.; Godoy Ponce, S.C.; Van Wittenberghe, S.; Verrelst, J.; Delegido, J. Spatial and Temporal Analysis of Water Quality in High Andean Lakes with Sentinel-2 Satellite Automatic Water Products. *Sensors* **2023**, *23*, 8774. [CrossRef]
52. Deutsch, E.S.; Cardille, J.A.; Koll-Egyed, T.; Fortin, M.-J. Landsat 8 Lake Water Clarity Empirical Algorithms: Large-Scale Calibration and Validation Using Government and Citizen Science Data from across Canada. *Remote Sens.* **2021**, *13*, 1257. [CrossRef]
53. Spyrakos, E.; O'Donnell, R.; Hunter, P.D.; Miller, C.; Scott, M.; Simis, S.G.H.; Neil, C.; Barbosa, C.C.F.; Binding, C.E.; Bradt, S.; et al. Optical types of inland and coastal waters. *Limnol. Oceanogr.* **2018**, *63*, 846–870. [CrossRef]
54. Neil, C.; Spyrakos, E.; Hunter, P.D.; Tyler, A.N. A global approach for chlorophyll-a retrieval across optically complex inland waters based on optical water types. *Remote Sens. Environ.* **2019**, *229*, 159–178. [CrossRef]
55. Mobley, C. *Light and Water: Radiative Transfer in Natural Waters*; Academic Press: New York, NY, USA, 1994; Volume 565.
56. Maciel, D.A.; Pahlevan, N.; Barbosa, C.C.F. Water Quality and Remote Sensing Reflectance Data for Global Inland, Coastal and Ocean Waters [Dataset]. PANGAEA. 2023. Available online: https://doi.pangaea.de/10.1594/PANGAEA.961720 (accessed on 4 November 2024).
57. Zhang, Y.; Shi, K.; Sun, X.; Zhang, Y.; Li, N.; Wang, W.; Zhou, Y.; Zhi, W.; Liu, M.; Li, Y.; et al. Improving remote sensing estimation of Secchi disk depth for global lakes and reservoirs using machine learning methods. *GIScience Remote Sens.* **2022**, *59*, 1367–1383. [CrossRef]
58. Khan, R.M.; Salehi, B.; Niroumand-Jadidi, M.; Mahdianpari, M. Mapping Water Clarity in Small Oligotrophic Lakes Using Sentinel-2 Imagery and Machine Learning Methods: A Case Study of Canandaigua Lake in Finger Lakes, New York. *IEEE J. Sel. Top. Appl. Earth Obs. Remote Sens.* **2024**, *17*, 4674–4688. [CrossRef]